Stanford Exploration Project, Report 113, July 8, 2003, pages 127–139

Multichannel deconvolution imaging condition for shot-profile migration

Alejandro A. Valenciano and Biondo Biondi[1]

ABSTRACT

A significant improvement of seismic image resolution is obtained by framing the shot-profile migration imaging condition as a 2-D deconvolution in the shot position/time (x_s, t) domain. This imaging condition gives a better image resolution than the crosscorrelation imaging condition and is more stable than the "more conventional" 1-D deconvolution imaging condition. A resolution increment is also observed in common image gathers (CIGs) computed with the 2-D deconvolution imaging condition, thus allowing a more accurate velocity analysis.

INTRODUCTION

Shot-profile migration is a method used to construct an image of the earth's interior from seismic data. This technique is implemented in two steps. The first step consists of constructing the source and the receiver wavefields for each shot position. This is done by downward propagation of an impulsive source and upward propagation of the data recorded at the surface. The second step consists of applying the imaging condition. The imaging step is based on Claerbout's imaging principle (Claerbout, 1971).

A practical way to implement Claerbout's imaging principle is to use match filters (crosscorrelation of the shot and receiver wavefields). Thereby, for each shot position, a partial image is obtained by matching the source and the receiver wavefields along the time dimension. Then, the image is formed by stacking the partial images at each subsurface location.

We propose a different imaging condition that also satisfies Claerbout's imaging principle. It consists of deconvolving the receiver wavefield by the source wavefield in the shot position/time (x_s, t) domain. This 2-D deconvolution imaging condition has the advantage of improving the image resolution while keeping the resulting image stable.

In this paper we show the advantages of the 2-D deconvolution over crosscorrelation and 1-D deconvolution imaging conditions. To do this, we use a synthetic model with five dipping reflectors. Using this model, we demonstrate the advantages of 2-D deconvolution not only for image resolution but also for estimating the correct moveout of reflectors in the angle-domain (Sava and Guitton, 2003).

[1]**email:** valencia@sep.stanford.edu, biondo@sep.stanford.edu

DATA AND WAVEFIELD DIMENSIONALITY

To implement a better imaging condition that is also feasible, it is important to understand 3-D prestack data and wavefield dimensionality. 3-D prestack seismic data are defined in a 5-D continuum (t, x_s, y_s, x_g, y_g) (Biondi, 1998), where t is time, x_s, y_s and x_g, y_g are the surface coordinates of the sources and the receivers, respectively.

After applying the first step of shot-profile migration (source and receiver wavefield construction) the dimensionality of the data increases. Thus, for each shot position (x_s, y_s) the source and the receiver wavefields $\mathbf{u}(x, y, z, t)$ and $\mathbf{d}(x, y, z, t)$ are defined in four dimensions (Figure 1), where (x, y, z) are the image space dimensions.

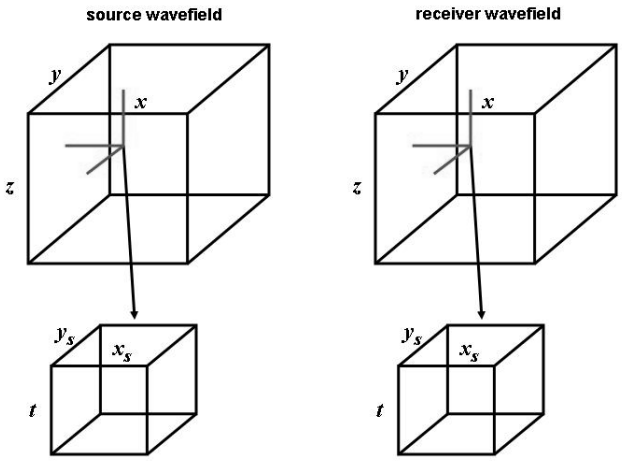

Figure 1: Data dimensionality. The source and receiver wavefields are 6-D datasets. alejandro1-match3 [NR]

In the following analysis, we explain how to combine the source and the receiver wavefields to obtain an image. For simplicity, we restrict our analysis to 2-D prestack data. In this case, the source and the receiver wavefields are 4-D datasets defined in (x, z, t) for each shot position x_s.

1-D IMAGING CONDITIONS

Claerbout's imaging principle

According to Claerbout's (1971) imaging principle, a reflector exists where the source and the receiver wavefields coincide in time and space. Claerbout expresses the imaging condition as follows:

$$\mathbf{r}(x, z) = \frac{\mathbf{u}(x, z, t_d)}{\mathbf{d}(x, z, t_d)}, \tag{1}$$

where x is the horizontal coordinate, z is the depth, and t_d is the time at which the source wavefield $\mathbf{d}(x, z, t_d)$ and the receiver wavefield $\mathbf{u}(x, z, t_d)$ coincide in time and space. This principle states that the reflectivity strength $\mathbf{r}(x, z)$ depends only on the source and the receiver

wavefields at time t_d. The time t_d is not known a priori, therefore we need a practical way to locate the reflector position in the (x,z) plane and compute its strength.

1-D Crosscorrelation

A practical way to compute the reflectivity strength in equation (1) is discussed in Claerbout (1971). He computes the reflector strength and position as the zero lag of the crosscorrelation of the source and the receiver wavefields in the time dimension (Figure 2).

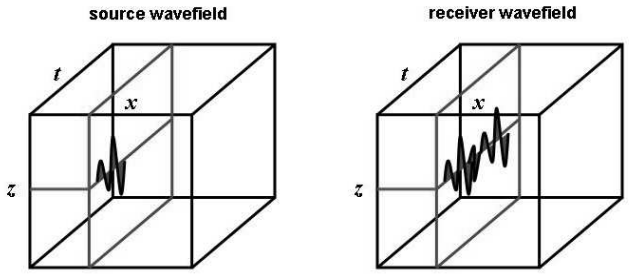

Figure 2: Source and receiver wavefields to be matched in the time dimension. alejandro1-match1 [NR]

The previous concept is expressed in the formula :

$$\mathbf{r}(x,z) = \sum_{x_s} \sum_{\omega} \mathbf{U}(x,z,\omega,x_s)\mathbf{D}^*(x,z,\omega,x_s), \tag{2}$$

where $\mathbf{r}(x,z)$ is the zero lag coefficient of the crosscorrelation, which is computed by summation over the frequencies and $\mathbf{U}(x,z,\omega)$ and $\mathbf{D}(x,z,\omega)$ are the one-dimensional Fourier Transforms of the receiver and the source wavefields, respectively. The contribution of each shot (located at x_s) is added to form the final image.

1-D Deconvolution

The division in equation (1) is better approximated by implementing a 1-D deconvolution imaging condition in the time dimension. It adds more complexity and potential instability in the computation of the image, but better approximates the definition of the reflection coefficient (ratio between incoming and reflected wave amplitude).

In practice, however, the 1-D deconvolution can be computed in the Fourier domain as a polynomial division. The zero lag coefficient is computed as the sum over frequencies:

$$\mathbf{r}(x,z) = \sum_{x_s} \sum_{\omega} \frac{\mathbf{U}(x,z,\omega,x_s)\mathbf{D}^*(x,z,\omega,x_s)}{\mathbf{D}(x,z,\omega,x_s)\mathbf{D}^*(x,z,\omega,x_s) + \varepsilon^2(x,z,x_s)}. \tag{3}$$

In equation (3), $\mathbf{U}(x,z,\omega)$ and $\mathbf{D}(x,z,\omega)$ are the one-dimensional Fourier transforms of the receiver and the source wavefields respectively. The contribution of each shot (located at x_s) is added to form the final image.

Notice that the regularization parameter $\varepsilon(x,z,x_s)$ can vary spatially. Jacobs (1982) discuss the difficulties of choosing a spatially variable ε. In practice, defining ε as a function of a dimensionless parameter λ makes its selection easier (Claerbout, 1991). We define this dependence as

$$\varepsilon^2(x,z,x_s) = \lambda < \mathbf{D}(x,z,\omega,x_s)\mathbf{D}^*(x,z,\omega,x_s) >, \tag{4}$$

where $<>$ indicates the mean in the frequency dimension. λ can be set constant for the whole image because it is independent of the data scale.

A 1-D imaging conditions implicitly make the assumption that each shot contributes to the image with the same weight [equations (2) and (3)]. This assumption is far from reality, since even when the subsurface geometry is not complex, reflectors are illuminated in a different way according to the source position.

2-D IMAGING CONDITIONS IN THE (X_S, T) PLANE

We can apply an imaging condition that does not assume a uniform contribution of the shots to the image. This can be done by framing the imaging condition as either a 2-D crosscorrelation or a 2-D deconvolution in the shot position/time dimensions (x_s,t). Figure 3 shows a cartoon of the domain where this imaging condition is computed. As showed in Figure 3, we can extract a plane (x_s,t) from the source and the receiver wavefields at each (x,z) position in the image.

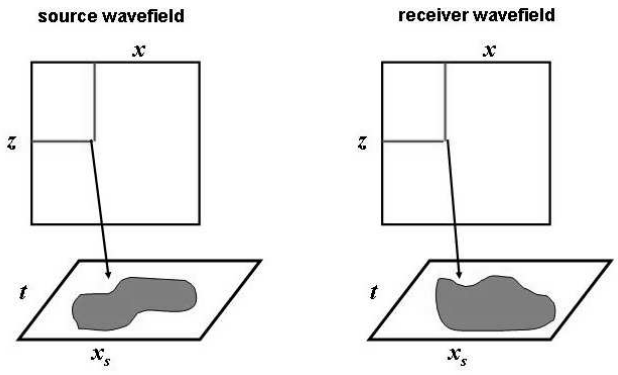

Figure 3: Source and receiver wavefields to be matched in the shot position/time plane. alejandro1-match2 [NR]

2-D crosscorrelation

The zero lag of the 2-D crosscorrelation of the source and the receiver wavefields in (x_s,t) is the same as the zero lag of the 1-D crosscorrelation in the time domain with a stack across the shot position axis. A simple example with matrices illustrates the concept. If we take the 2-D crosscorrelation of 2 matrices,

$$\begin{bmatrix} 1 & 2 \\ 2 & 3 \end{bmatrix} \star\star \begin{bmatrix} 4 & 1 \\ 2 & 5 \end{bmatrix} = \begin{bmatrix} 12 & 14 & 4 \\ 11 & 25 & 12 \\ 2 & 11 & 5 \end{bmatrix}, \tag{5}$$

the zero lag coefficient is 25. If instead we crosscorrelate the columns,

$$\begin{bmatrix} 1 \\ 2 \end{bmatrix} \star \begin{bmatrix} 4 \\ 2 \end{bmatrix} = \begin{bmatrix} 8 \\ 8 \\ 2 \end{bmatrix} \tag{6}$$

$$\begin{bmatrix} 2 \\ 3 \end{bmatrix} \star \begin{bmatrix} 1 \\ 5 \end{bmatrix} = \begin{bmatrix} 3 \\ 17 \\ 10 \end{bmatrix} \tag{7}$$

take the zero lag, and stack over the rows, the result is also 25. This illustrates the relationship that exists between the 1-D and the 2D crosscorrelation.

2-D deconvolution

In the case of deconvolution, the relation between 2-D and 1-D (plus stacking), if it exists, is not straightforward to illustrate. This is because deconvolution in the (x_s, t) plane should be implemented by recursive filtering. However, we know that 2-D deconvolution in the (x_s, t) plane compresses the information in both the shot and the time dimensions. This is a better way of compressing information than 1-D deconvolution followed by a stack in the shot dimension.

In practice, however, 2-D deconvolution can be computed as a polynomial division in the Fourier domain. But in this case, the wavefields that are divided, $\mathbf{U}(x,z,\omega,k_{x_s})$ and $\mathbf{D}(x,z,\omega,k_{x_s})$, are the two-dimensional Fourier transforms of the receiver and the source wavefields, respectively.

The zero lag coefficient of the 2-D deconvolution is computed as:

$$\mathbf{r}(x,z) = \sum_{k_{x_s}} \sum_{\omega} \frac{\mathbf{U}(x,z,\omega,k_{x_s})\mathbf{D}^*(x,z,\omega,k_{x_s})}{\mathbf{D}(x,z,\omega,k_{x_s})\mathbf{D}^*(x,z,\omega,k_{x_s}) + \varepsilon^2(x,z)}. \tag{8}$$

Note that whereas we sum over the shot positions (x_s) in equation (3), we now sum over the shot position spatial frequency (k_{x_s}) in equation (8).

Also notice that the regularization parameter $\varepsilon(x,z)$ is spatially variable but constant in the (ω, k_{x_s}) plane. It is defined as

$$\varepsilon^2(x,z) = \lambda < \mathbf{D}(x,z,\omega,k_{x_s})\mathbf{D}^*(x,z,\omega,k_{x_s}) > \tag{9}$$

where $<>$ is the mean in the (ω, k_{x_s}) plane.

Analogous to Rickett and Sava (2000), we extend the 2-D deconvolution imaging condition to compute a range of offsets. This is done by shifting the source and the receiver wavefields in the x dimension. Then, the nonzero-offset reflectivity can be computed as follows:

$$\mathbf{r}(x,z,h) = \sum_{k_{x_s}} \sum_{\omega} \frac{\mathbf{U}(x-h,z,\omega,k_{x_s})\mathbf{D}^*(x+h,z,\omega,k_{x_s})}{\mathbf{D}(x+h,z,\omega,k_{x_s})\mathbf{D}^*(x+h,z,\omega,k_{x_s}) + \varepsilon^2(x+h,z)}. \tag{10}$$

where h is the subsurface offset.

In the following section we show the advantages of 2-D deconvolution imaging condition over the crosscorrelation and the 1-D deconvolution imaging conditions.

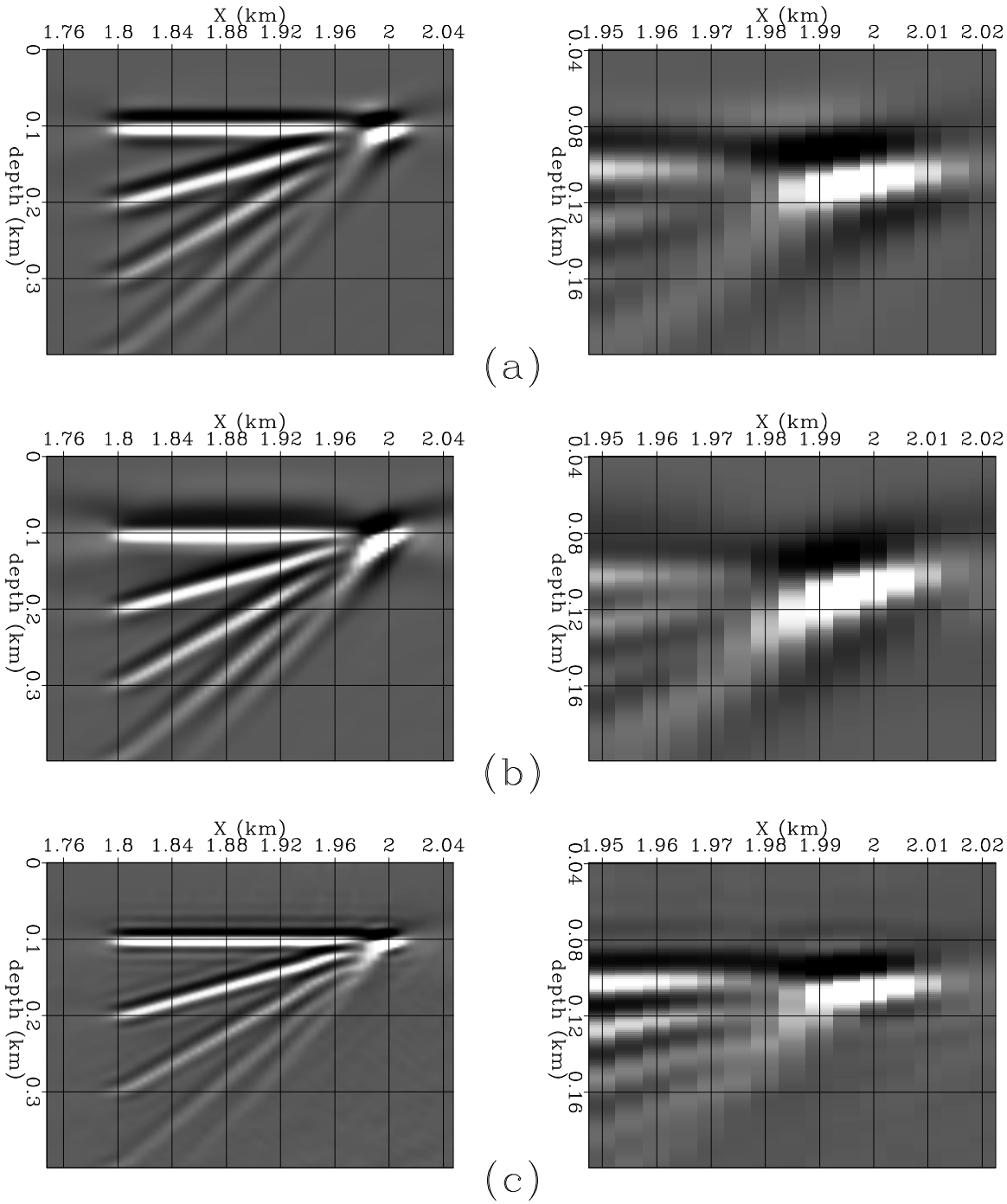

Figure 4: Comparison of 3 different imaging conditions.(a) Image obtained with the crosscorrelation imaging condition. (b) Image obtained with the 1-D deconvolution imaging condition in the time dimension. (c) Image obtained with the 2-D deconvolution imaging condition in the (x_s, t) dimensions. alejandro1-mig_tune2 [CR]

RESULTS WITH SYNTHETIC DATA

Zero offset image resolution

To compare the result of the different imaging conditions, we build a constant velocity model of five dipping layers pinching-out to the right of the model. The deepest reflector has the steepest dip angle ($\approx 63°$) and the shallowest has zero dip. Figure 4 shows a comparison of three different imaging conditions. Figure 4a uses the crosscorrelation imaging condition, Figure 4b the 1-D deconvolution imaging condition along the time dimension ($\lambda = 0.05$) and Figure 4c the 2-D deconvolution imaging condition in the (x_s, t) plane ($\lambda = 0.05$). Notice the better resolution of the 2-D deconvolution image.

The better stability of the 2-D deconvolution image is demonstrated by comparing Figure 5 and Figure 6. They display the result of the 1-D deconvolution and the 2-D deconvolution for different λ values at a fixed x position (1.96 km in Figure 4).

Notice that when λ decreases, the 1-D deconvolution result presents low frequency noise. The stacking across the shot position [equation (3)] reduces the high frequency noise but might increase some low spatial frequency noise that is periodic with the shot positions. In the case of 2-D deconvolution, when λ decreases, the noise contaminates the image in all the spatial frequency bandwidth. However, the signal to noise ratio for this imaging condition is much higher than for the 1-D deconvolution imaging condition.

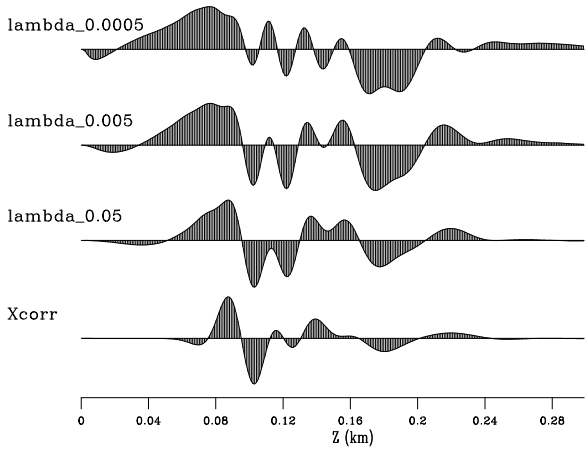

Figure 5: Effect of lambda on 1-D deconvolution. From bottom to top: crosscorrelation, $\lambda = 0.05$, $\lambda = 0.005$ and $\lambda = 0.0005$ alejandro1-Comp_1d_epsst [CR]

From this results, we can conclude that the 2-D deconvolution imaging condition in the (x_s, t) plane gives a better resolution than the other imaging conditions. The 2-D deconvolution final image is less sensitive to the choice of λ and is less affected by the low frequency noise visible in the 1-D deconvolution result. The less sensitivity to λ choice is important, since deconvolution major handicap is the selection of the regularization parameter.

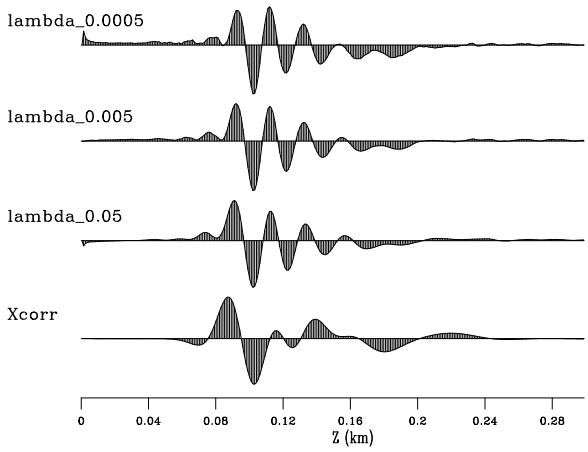

Figure 6: Effect of lambda on 2-D deconvolution. From bottom to top: crosscorrelation, $\lambda = 0.05$, $\lambda = 0.005$ and $\lambda = 0.0005$ alejandro1-Comp_epsst [CR]

CIGs and velocity analysis resolution

Not only the zero-offset image resolution is important. Having a better image resolution for a range of offsets and angles can lead to better estimation of the reservoir properties and better velocity analysis. The angle-domain Common Image Gather (CIG) is the domain where AVA analysis is performed, because it has information about the reflectivity variation with angle (Shuey, 1985). Angle-domain CIGs have also information about how well events are focused at depth, thus providing a natural domain for migration-focusing velocity analysis (Biondi and Sava, 1999).

Following equation (10), we compute offset-domain CIGs with the 2-D deconvolution imaging condition. Figure 7a shows the offset-domain CIGs computed with the 1-D cross-correlation imaging condition. As expected, they show less resolution than the offset-domain CIGs computed with the 2-D deconvolution imaging condition (Figure 7c).

We transform offset-domain CIGs into angle-domain CIGs following the method presented by Sava and Fomel (2000). Figure 7b shows the angle-domain CIGs computed with the 1-D crosscorrelation imaging condition. They also show less resolution than the angle-domain CIGs computed with the 2-D deconvolution imaging condition (Figure 7d).

We now compare the previous gathers with the gathers resulting from the migration of the data with a 3% lower velocity. Figures 8a to 8d display the offset-domain and the angle-domain CIGS computed with the 1-D crosscorrelation imaging condition and the 2-D deconvolution imaging conditon for the low velocity, respectively. Notice that with the 2-D deconvolution the curvature of the events, due to the low migration velocity, appears more clear.

Finally, we use the angle-domain Radon transform (ART) methodology described in Sava and Guitton (2003) to estimate the curvature of the reflectors in the angle-domain CIGs. Since the curvature of the reflectors in the ART domain is related to velocity errors, a better curvature estimation can lead to a better velocity estimation. A flat reflector in the angle-domain CIG maps at zero q (curvature index) in the ART CIGs. Conversely, a reflector with moveout in the angle-domain CIG should map away from zero q in the ART CIG.

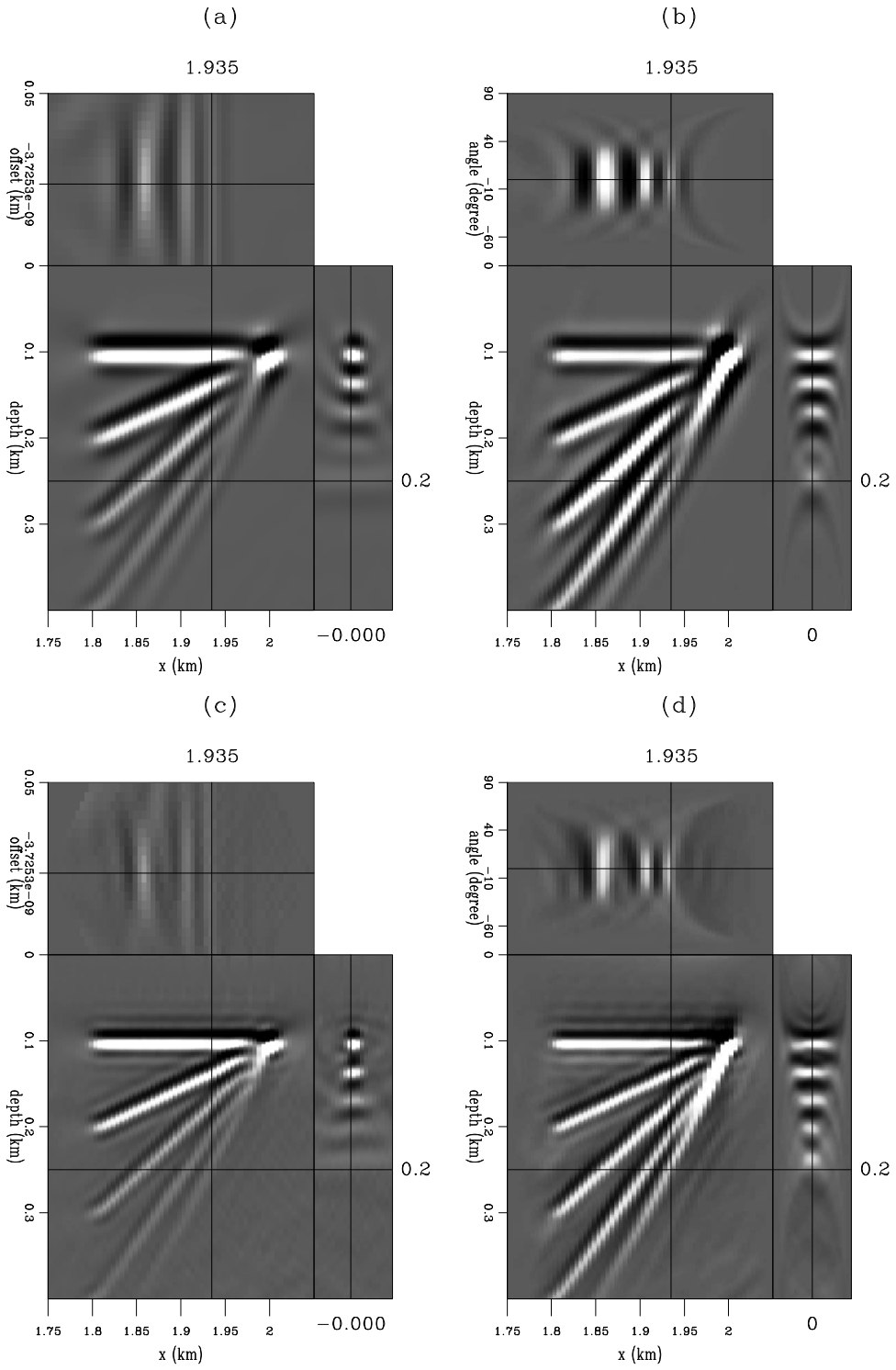

Figure 7: Comparison between 1-D crosscorrelation and 2-D deconvolution imaging conditions. (a) 1-D crosscorrelation offset-domain CIGs. (b) 1-D crosscorrelation angle-domain CIGs. (c) 2-D deconvolution offset-domain CIGs. (d) 2-D deconvolution angle-domain CIGs. alejandro1-Comp_tune_stn [CR]

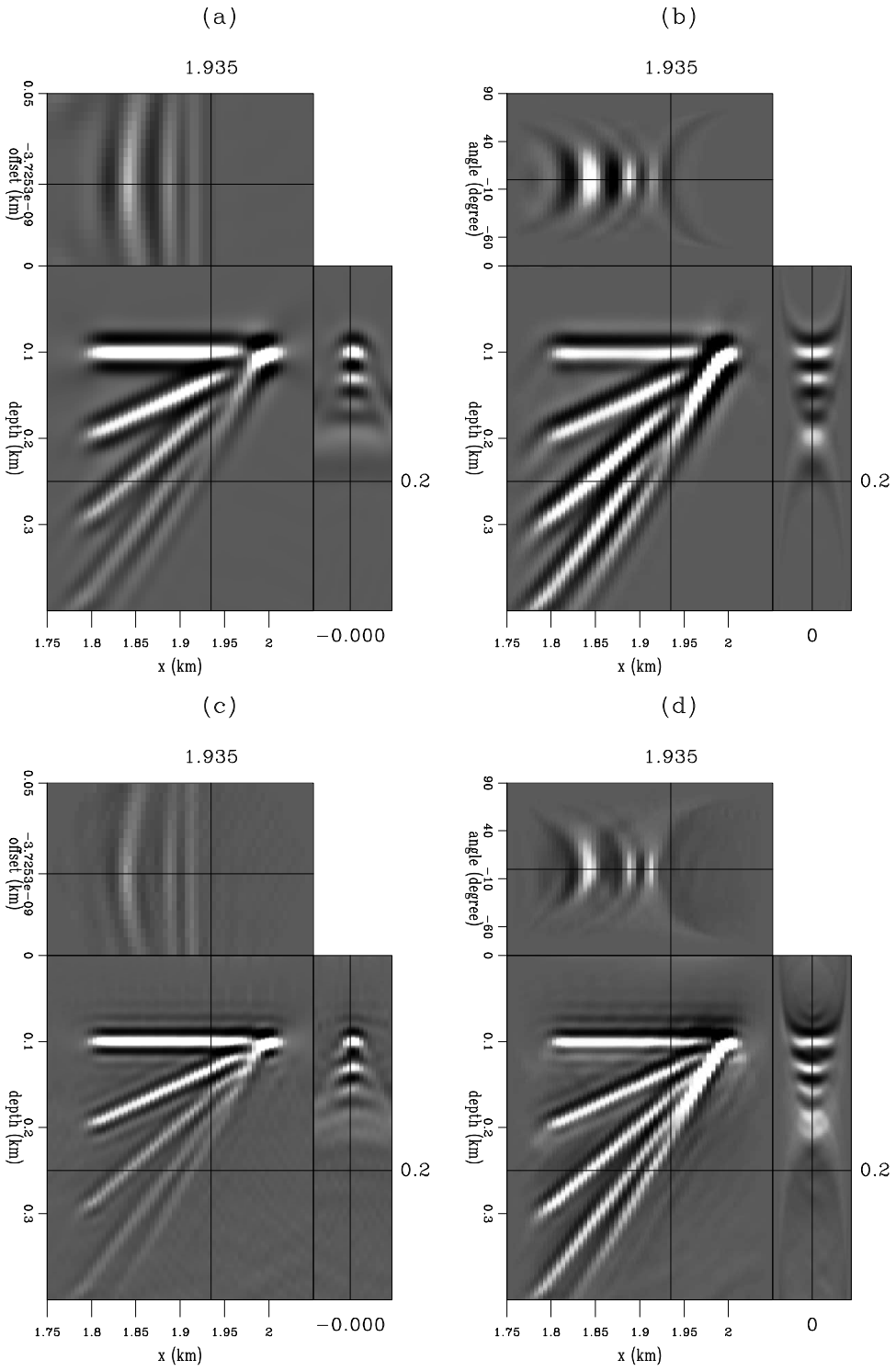

Figure 8: Comparison between 1-D crosscorrelation and 2-D deconvolution imaging conditions for a 3% lower velocity. (a) 1-D crosscorrelation offset-domain CIGs. (b) 1-D crosscorrelation angle-domain CIGs. (c) 2-D deconvolution offset-domain CIGs. (d) 2-D deconvolution angle-domain CIGs. alejandro1-Comp_tune_stn3low [CR]

In Figure 9 we compare the ART CIGs with the correct velocity (Figure 9a and Figure 9b) and the low velocity (Figure 9c and Figure 9d). In both cases we calculated the angle-domain CIGs with 1-D crosscorrelation (Figure 9a and Figure 9c) and 2-D deconvolution (Figure 9b and Figure 9d).

Notice that 2-D deconvolution imaging condition gives ART CIGs that are easier to interpret. Also notice that due to the lack of resolution, ART CIGs computed with 1-D crosscorrelation and the correct velocity Figure (9a) show events that can be misinterpreted as reflectors with the wrong velocity. In addition, ART CIGs computed with 1-D crosscorrelation and the wrong velocity Figure (9c) show events that can be misinterpreted as reflectors with the correct velocity. This problem is reduced with the 2-D deconvolution imaging condition (Figure 9b and Figure 9d) .

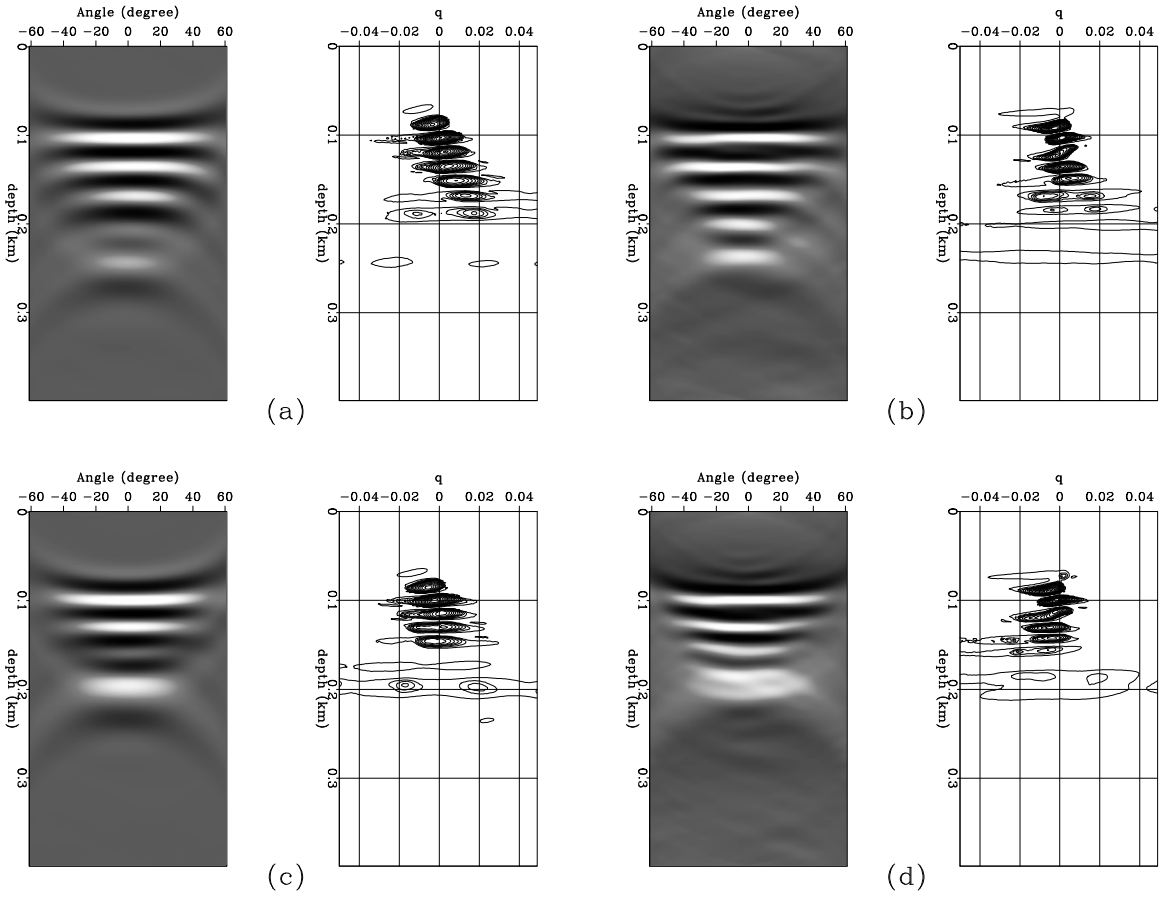

Figure 9: Comparison between the 1-D crosscorrelation and the 2-D deconvolution imaging conditions for the correct and the low velocity. (a) Angle-domain and ART CIGs computed with the 1-D crosscorrelation and the correct velocity. (b) Angle-domain and ART CIGs computed with the 2-D deconvolution and the correct velocity. (c) Angle-domain and ART CIGs computed with the 1-D crosscorrelation and the low velocity. (d) Angle-domain and ART CIGs computed with the 2-D deconvolution and the low velocity. alejandro1-test-art-mig [CR]

CONCLUSIONS

By framing the shot-profile migration imaging condition as a 2-D deconvolution in the (x_s, t) plane the final image resolution is enhanced. The 2-D deconvolution gives better resolution than the crosscorrelation and the 1-D deconvolution imaging conditions.

The 2-D deconvolution imaging condition gives also a more robust result than the 1-D deconvolution imaging condition because it is less dependent on the regularization parameter and it is less affected by the low frequency noise. This is an important property of the 2-D deconvolution, since one deconvolution application major handicap is the selection of the regularization parameter.

In addition, the angle-domain CIGs computed with the 2-D deconvolution imaging condition are less affected by low resolution effects. Consequently, we can estimate better velocities with migration-focusing velocity analysis.

ACKNOWLEDGMENTS

The authors thank Guojian Shan and Brad Artman for providing the programs to construct the source and the receiver wavefields. We also thank Paul Sava, Antoine Guitton, and Gabriel Alvarez for their important suggestions.

REFERENCES

Biondi, B., and Sava, P., 1999, Wave-equation migration velocity analysis: SEP–**100**, 11–34.

Biondi, B., 1998, 3-D seismic imaging: SEP–**98**, 1–204.

Claerbout, J. F., 1971, Toward a unified theory of reflector mapping: Geophysics, **36**, no. 3, 467–481.

Claerbout, J. F., 1991, Earth Soundings Analysis: SEP–**71**, 1–304.

Jacobs, B., 1982, The prestack migration of profiles: SEP–**34**.

Rickett, J. E., and Sava, P. C., 2000, Offset and angle-domain common image-point gathers for shot-profile migration: Geophysics, **67**, no. 03, 883–889.

Sava, P., and Fomel, S., 2000, Angle-gathers by Fourier Transform: SEP–**103**, 119–130.

Sava, P., and Guitton, A., 2003, Multiple attenuation in the image space: SEP–**113**, 31–44.

Shuey, R. T., 1985, A simplification of the zoeppritz-equations:, **50**, no. 04, 609–614.